

Elastic and inelastic processes in $H^+ + CH_4$ collisions in the low-kilo-electron-volt regime

M. Kimura

*Argonne National Laboratory, Argonne, Illinois 60439
and Department of Physics, Rice University, Houston, Texas 77251*

Y. Li, G. Hirsch, and R. J. Buenker

Theoretische Chemie, Bergische Universität-Gesamthochschule Wuppertal, D-42097 Wuppertal, Germany

(Received 14 July 1994; revised manuscript received 13 April 1995)

Electron capture and direct elastic scattering in collisions of H^+ ions with CH_4 molecules are studied by using a molecular representation within a fully quantum-mechanical approach below 1.5 keV. Calculations are carried out at two different molecular configurations: (i) C_{3v} symmetry, in which H^+ approaches along the direction of a C—H in CH_4 , and (ii) C_{2v} symmetry, in which H^+ approaches along a bisector of a H—C—H bond angle. We find that electron capture in the C_{2v} symmetry configuration takes place preferentially over that in the C_{3v} symmetry configuration at scattering angles below 15° at 1.5 keV, and that the situation reverses at larger scattering angles. Hence, interferences arising from these molecular configurations on differential cross sections for electron capture and elastic scattering processes are present but weak, except for angles near the crossing. Accordingly, the total cross section for the C_{2v} symmetry is larger by more than an order of magnitude, because in this symmetry H^+ can penetrate deep inside the electron distribution of the CH_4 molecule, causing a strong interaction. In addition, angular dependence in the differential cross section is quite different for the two molecular configurations at all energies studied.

PACS number(s): 34.70.+e, 34.20.-b, 34.50.-s

I. INTRODUCTION

Electron capture in collisions of ions with atoms in the low-keV energy regions has been one of the most active research areas, experimentally and theoretically, in atomic physics in the last two decades, because it provides fundamental information for atomic and molecular spectroscopy and many-body collision dynamics. The study of electron capture is also important for applications like astrophysics and fusion research. Comparatively comprehensive studies involving a variety of atomic targets, a wide range of collision energies (meV to keV), and various charged projectiles have greatly improved our understanding of electron capture in ion-atom collisions [1,2]. An increasing volume of cross-section data for electron capture is now available for application. Unlike studies of atomic targets, both experimental and theoretical studies of molecular targets are scarce, although molecular targets are as important as atomic targets in basic as well as applied sciences. The complexity in theoretical approaches for treating molecules might cause this subfield to be rather inactive compared to its atomic counterpart. Only for the H_2 target have limited but relatively extensive studies of the molecular effects on electron capture been reported to date [3–8], and no similar level of theoretical study has been carried out for other molecular targets.

One of the important polyatomic molecules urgently requiring study for an understanding of collision dynamics and for compilation of a set of cross-section data is CH_4 (methane), which is abundant in various astrophysical environments, fusion reactors, and plasma chemistry

atmospheres where various types of charged particles constantly interact with it. A recent report [9] suggested that various protoamino acids produced as a result of high-energy proton irradiation of a simulated primitive earth atmosphere (a mixture of methane, nitrogen, and water) may be important clues in understanding the origin of life on earth. As for dynamics, only some exploratory experimental studies have been reported on electron capture. Among those are measurements of electron capture in the keV regime [10,11], a recent experimental study specifically on the fragmentation of CH_4 resulting from electron capture by proton impact at 4 MeV [12] and a measurement of differential cross sections for direct elastic scattering and electron capture for scattering angles up to 0.1° at 1.5 keV, in connection with atmospheric physics [13]. Below 50 eV, a series of careful studies of inelastic and charge-transfer processes resulting from ion-molecule collisions using a crossed-beam experiment was carried out by Toennies and co-workers [14–16]. In particular, a study of the present collision system by Chiu *et al.* [16], combined with a theoretical analysis based on the correlation diagram, reveals details of electron capture and fragmentation mechanisms in this low-energy regime. At near-thermal energies, where electron-capture processes are important for chemical models of the planetary atmosphere, rate coefficients for the process were estimated to be less than 5×10^{-9} cm³/s below 300 K [17].

In this paper, we report electron capture and direct elastic scattering resulting from collisions of H^+ ions with CH_4 molecules below 1.5 keV. We obtain our results by using a molecular-orbital expansion method

within a fully quantum-mechanical formalism. Three molecular configurations are specifically considered to study the effects of molecular orientations on collision dynamics: (i) a proton approaches the H atom in a C—H bond; (ii) it comes along the same line as in (i) but in the opposite direction, passing through the center of an H_3 triangle (C_{3v} face-centered approach); and (iii) a proton approaches along the bisector of an H—C—H bond angle (directly facing the C atom in the center of CH_4). While knowledge of these molecular configurations is not sufficient to give detailed information about vibrational structure and geometrical relaxation effects, it should be enough to allow for reliable predictions of cross sections for elastic and inelastic processes that occur as a result of collisions with intermediate energies (\sim keV) for which the Franck-Condon principle is valid; that is, for interaction times (10^{-16} – 10^{-15} s) of colliding particles that are small compared to relevant vibrational periods of CH_4 (ca. 10^{-14} s and longer). Thus in what follows the geometrical conformation of the methane target is held fixed to that observed under conditions of thermodynamic equilibrium. The interference arising from different approaches of the proton to the CH_4 molecule is investigated, however. This study sheds light on the dynamics of the molecular orientation effect and provides guidelines for developing a simple model to describe a complex polyatomic molecular target. Furthermore, the interferences of various origins are an interesting subject of basic physics, and they form an essential basis for possible use of this technique for material and surface analysis.

II. THEORETICAL MODEL

The theoretical methods used here are standard and have been described in detail elsewhere [1]. Hence, only a brief summary is provided here.

A. Molecular states

The adiabatic potential-energy curves are calculated by means of the multireference single- and double-excitation configuration-interaction method [18], with configuration selection and energy extrapolation employing the Table-CI algorithm [19] for efficient handling of Hamiltonian matrix elements for many-electron basis functions (symmetrized linear combinations of Slater determinants). The atomic-orbital (AO) basis used for carbon consists of the $(9s5p1d)$ primitive set of Huzinaga [20], contracted to $[5s3p1d]$ by Dunning [21], with additional Rydberg functions of the s and p types ($\alpha_s=0.023$, $\alpha_s=0.0055$, $\alpha_p=0.021$, $\alpha_p=0.0049$). The hydrogen basis (from the same authors) is $(5s1p)$ contracted to $[3s1p]$.

The calculations are carried out in two different point groups, depending on the approach of the proton toward the methane molecule. In the approach along the direction of a C—H bond, the systems have overall symmetry of C_{3v} , with calculations done in C_s , the highest corresponding Abelian subgroup of C_{3v} . If H^+ approaches along a bisector of an H—C—H bond angle, the overall symmetry is C_{2v} , and the calculations are performed in this point group. It should be noted that the effects of a

proton approaching perpendicular to an H_3 face of the methane tetrahedron (also C_{3v} symmetry, the opposite of the approach along the C—H bond, denoted as the C_{3v} face in the subsequent discussion) are not greatly different than those for the three C_{2v} trajectories (considered explicitly in the present treatment) that bisect each of the HH internuclear separations, forming the corresponding equilateral triangles.

The CI treatment is based on all configurations that are generated by making either single or double orbital substitutions with respect to a number of key or reference configurations. The resulting generated set is divided into groups of strongly and weakly interacting configurations, respectively, on the basis of the value of the second-order perturbative energy lowering (ΔE_j) in each case. A selection threshold T is used to separate the configurations into these two categories. In the present case this threshold has an energy value of $T=5.0 \mu\text{hartree}$. The multireference analog of the Davidson correction [19], namely $(1 - \sum_p c_p^2)(E_{CI} - E_{ref})$, where $\sum_p c_p^2$ is the sum of the squares of all coefficients of reference configurations in the final CI wave function, E_{CI} is the corresponding total energy, and E_{ref} is the corresponding energy obtained from the small secular equation involving only the reference configurations, is applied to estimate the full CI energy for each state in the AO basis employed.

In the practical calculation of eigenvalues and eigenfunctions, all coordinates within the CH_4 molecule were frozen at the equilibrium intramolecular distances of the tetrahedral geometry: $r_{C-H}=1.094 \text{ \AA}$ and $\theta_{H-C-H}=109.47^\circ$. Hence, only the internuclear distance (R) between the H^+ projectile and the C in CH_4 was varied. This approximation should be valid when the collision time is shorter than the vibrational period of the target molecule. In the present case, the approximation is reasonable down to a few tens of eV of collision energy. The justification for this conclusion is basically the same as for the Franck-Condon principle in electronic transitions taking place within a molecule. Furthermore, the geometry of the CH_4^+ molecular ions formed after electron capture is also frozen at the initial configuration, since including a relaxation of this approximation has little effect on electron-capture dynamics.

B. Collision dynamics

Collision dynamics are studied on the basis of the fully quantum-mechanical formulation of a molecular-orbital expansion method in which dynamical transitions are driven by nonadiabatic couplings [1]. The total scattering wave function is described in an adiabatic representation as an expansion in products of electronic and nuclear wave functions and the electron translation factor. Substitution of the total scattering wave function into the stationary Schrödinger equation yields coupled, second-order differential equations for nuclear wave function $X^a(R)$. It is computationally convenient to solve the coupled equations in a diabatic representation [1]. The transformation from the adiabatic to the diabatic representation can be readily achieved through a unitary

transformation matrix, $C(R)$. In this representation the nuclear wave function for the heavy particles is related to $X^d(R) = CX^a(R)$, and the diabatic potential matrix is $V^d = C^{-1}V^aC$, where V^a is the adiabatic potential matrix. The resulting coupled equations for $X^d(R)$ are given in matrix form as

$$\left[\frac{1}{2\mu} \nabla_R^2 I - V^d(R) + EI \right] X^d(R) = 0, \quad (1)$$

where μ is the reduced mass of the system, I is the identity matrix, and V^d is the diabatic matrix. The coupled equations (1) are solved numerically to obtain the scattering S^l matrix for each partial wave l . The differential cross section is then obtained from the standard formula

$$\frac{d\sigma(\theta)}{d\Omega} = \frac{1}{4k^2} \left[\sum_l (2l+1) \{ \delta_{if} - S_{if}^l \} P_l(\cos\theta) \right]^2, \quad (2)$$

where S_{if}^l is the scattering S -matrix element for partial wave l , θ is the scattering angle in center-of-mass coordinates, and k is the momentum of the projectile with collision energy $E = k^2/2$. Integration over all angles gives the total cross section. In the present calculation, we employed two- and three-state close-coupling treatments with molecular orbitals (MOs) corresponding to the initial ($H^+ + CH_4$) and electron-capture ($H + CH_4^+$) channels.

C. Analysis of oscillatory structures in the cross sections

For some systems, differential cross sections and sometimes total cross sections display oscillatory structures as functions of collision energy or scattering angle. A semiclassical analysis for these structures would be sound and would improve understanding of the underlying physics [22]. To discuss the scattering pattern, the deflection function $\Theta_J(L, E)$ must be determined for each trajectory and potential region J . This function is expressed as

$$\Theta_J(L, E) = \pi - 2b \int_{R_t}^{\infty} \left[1 - \frac{V(R)}{E} - \frac{b^2}{R^2} \right]^{-1/2} \frac{dR}{R^2}, \quad (3)$$

where b is the impact parameter and R_t is the inner zero (turning point) of the integrand. The parameter b relates to the orbital angular momentum L as

$$L^2 = 2\mu[E - V(\infty)]b^2, \quad (4)$$

where the classical mechanical quantity is connected to that of quantum mechanics. We carried out the semiclassical analysis to identify the origin of structures in differential cross sections whenever necessary as discussed below.

III. RESULTS

A. Adiabatic potentials and couplings

Adiabatic potential curves obtained by the procedure outlined in Sec. II A for C_{2v} and C_{3v} symmetries are displayed in Figs. 1(a) and 1(b), respectively. The

lowest level in the figures is the initial state dissociating to the electronic configuration [$H^+ + CH_4(^1A_1: 2a_1^2 t_{2a}^2 1t_{2b}^2 1t_{2c}^2)$]. The next group contains the ground electron-capture states corresponding to the electronic configuration [$H(1s) + CH_4^+(^2T_2: 2a_1^2 1t_{2a}^2 1t_{2b}^2 1t_{2c}^2)$]. Electronic excited ($H^+ + CH_4^*$) and ($H(2s) + CH_4^+$) states follow. In the infinite separation of internuclear distance between the projectile and the CH_4 molecule, the energy defects be-

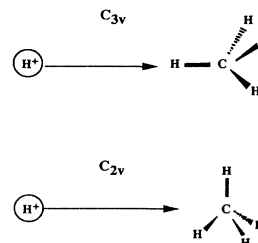
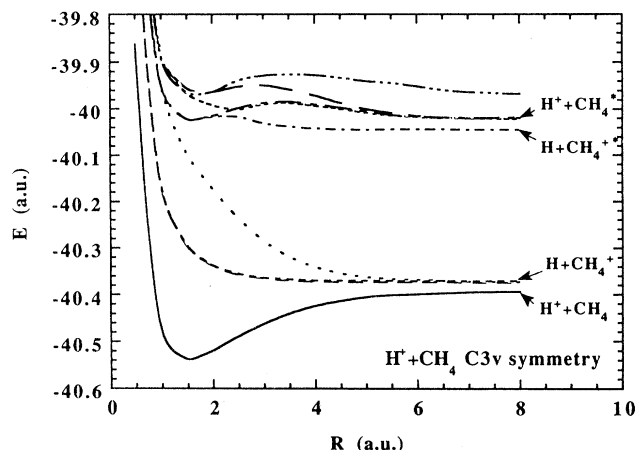
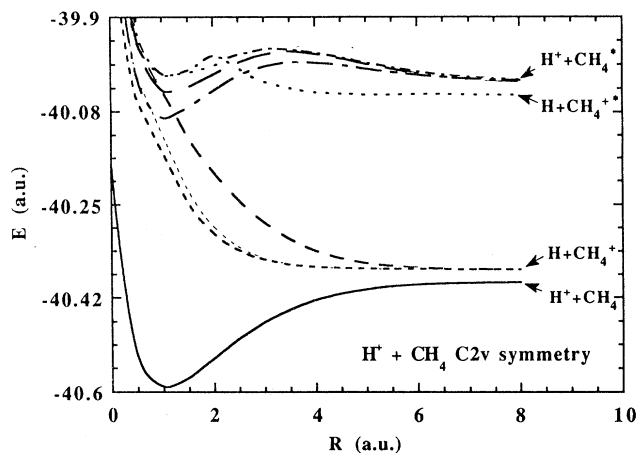


FIG. 1. (a) Adiabatic potential curves for C_{2v} symmetry. (b) Adiabatic potential curves for C_{3v} symmetry. (c) Schematic diagram indicating the molecular configurations for collisions.

tween the initial and electron-capture channels for both symmetries should be equal. However, at finite separations, these values are different. That for the C_{3v} symmetry is somewhat smaller, with a value of 0.021 27 a.u. at $R=10$ a.u., compared to 0.022 39 a.u. for C_{2v} symmetry at the same distance. The initial channel has a configuration mixing with the electron-capture channel at $R=1.0$ a.u. in C_{2v} symmetry, but no obvious mixing of electronic states is found for C_{3v} symmetry. Consideration of the molecular configuration [Fig. 1(c)] indicates that the H^+ ion can penetrate deep inside of the CH_4 molecule, causing vigorous mixing of electronic states. General shapes of the potential curves for C_{2v} and C_{3v} symmetries are similar, and a constant energy separation at finite R between the initial and electron-capture channels suggests that the collision dynamics are governed mainly by the Demkov-type coupling scheme at finite R [1]. Note that adiabatic potential curves for C_{3v} -face symmetry are closer to those of C_{2v} symmetry in nature except for somewhat stronger mixing at $R=1.0$ a.u. because of the similarity of the molecular configuration.

The dominant radial couplings are illustrated in Fig. 2. As we speculated above, the coupling in C_{2v} symmetry shows double peaks, namely, the narrow peak at $R=1.0$ a.u. followed by the broader peak at larger R . The first peak at $R=1.0$ a.u. is probably due to the localized electron density of H atoms. The presence of the second broad peak, which typically results from the Demkov-type coupling scheme near $R=5.5$ a.u. in C_{2v} symmetry, is noteworthy. Unlike C_{2v} symmetry, the coupling for C_{3v} symmetry is a single broad peak at $R < 4$ a.u., again as a consequence of the Demkov-type coupling scheme. This is because the incoming H^+ ions are affected little by the electronic field, except that of the H atom, which the incoming projectile approaches. This conspicuous difference in the couplings from different molecular configurations is significant and may well underscore a difference in the collision dynamics. The radial coupling for C_{3v} -face symmetry shares similar characteristics to that for C_{2v} symmetry, i.e., double peaks, but the first

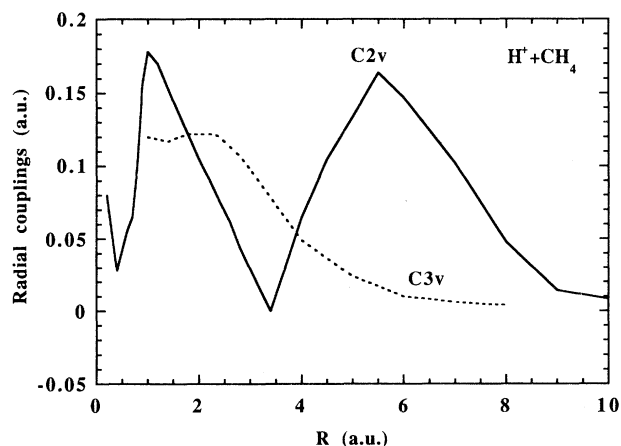


FIG. 2. Representative radial couplings between the initial and electron-capture states.

peak at $R=1.0$ a.u. is much larger, reflecting a stronger configuration mixing than that in C_{2v} symmetry.

B. Differential cross sections at high energies (> 100 eV)

1. General features

The differential cross sections obtained are shown in Figs. 3(a) and 3(b) for C_{2v} symmetry and Figs. 4(a) and 4(b) for C_{3v} symmetry, for scattering angles 0° – 180° at 1.5 and 0.5 keV, respectively. Both electron capture and direct elastic scattering are included. Several important features are summarized here and are discussed separately for small and large scattering angle regions: (i) $0^\circ \leq \theta < 20^\circ$ and (ii) $\theta \geq 20^\circ$.

First for $0^\circ \leq \theta < 20^\circ$, the magnitude of the differential cross sections for electron capture for C_{3v} symmetry is larger than that for C_{2v} symmetry in this scattering angle domain, except for a very small scattering angle region.

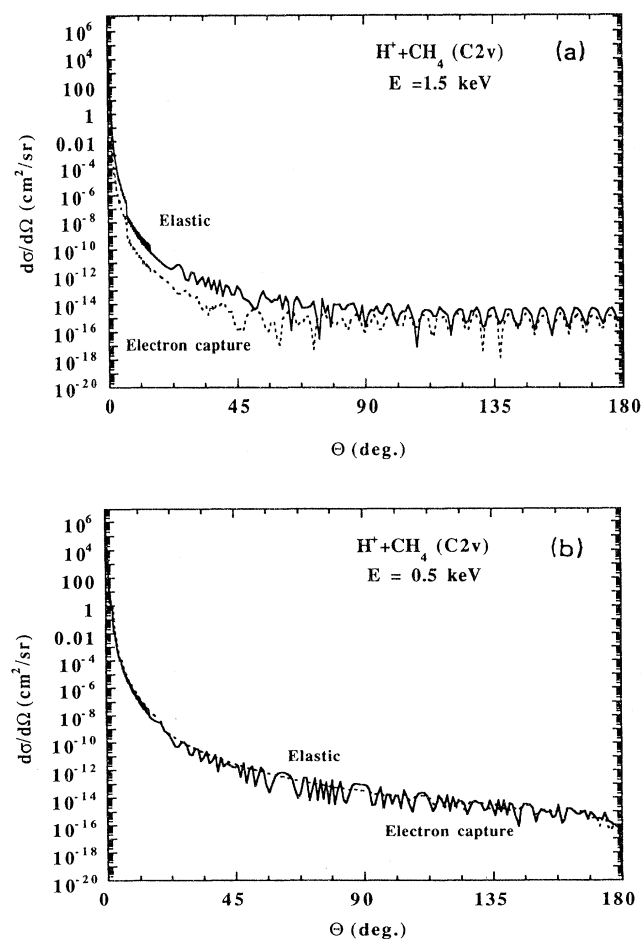


FIG. 3. (a) Differential cross section for C_{2v} at 1.5 keV. Solid line, elastic scattering; dashed line, electron capture. (b) Differential cross section for C_{2v} at 0.5 keV. Solid line, elastic scattering; dashed line, electron capture.

Below 0.5° , C_{2v} symmetry is far more dominant, by an order of magnitude. Events resulting in scattering angles of 10° or smaller correspond roughly to those of impact parameters larger than 2.0 a.u. At these large impact parameters, the projectile interacts only weakly with the constituent atoms in C_{2v} symmetry, because of limited effective formation of the molecular configuration. In contrast, the projectile may "feel" an isotropic field on its way out through three H atoms aligned with a 120° separation for C_{3v} symmetry. Interestingly, as we shall see later, the total electron-capture cross sections above 100 eV are larger by about two orders of magnitude for C_{2v} symmetry than for C_{3v} symmetry. This is because the near-zero angle scattering controls most of the total cross section. In addition, the small, high-frequency oscillations that are apparent for C_{3v} symmetry in both elastic and electron-capture differential cross sections may be attributable to quantum interferences. For C_{2v} symmetry, oscillatory structures are present, but they are much weaker and are irregular.

Second, for $\theta \geq 20^\circ$, both elastic and electron-capture

differential cross sections are smooth and flat with a near-constant value of 10^{-3} cm²/sr as a function of scattering angles (i.e., isotropic scattering) for C_{3v} symmetry, while those for C_{2v} symmetry have numerous irregular oscillations with very small mean values of 10^{-14} cm²/sr. These oscillations in C_{2v} symmetry are due to quantum interferences arising from two-state strong coupling. For C_{3v} symmetry, the isotropy is due to near head-on collisions between the projectile and the H atom in CH₄. One remarkable feature, a sharp dip in electron capture at 45° for 1.5 keV and 75° for 0.5 keV, is considered to be due to rainbow scattering. For $\theta \geq 20^\circ$, elastic scattering is nearly comparable in magnitude to electron capture for C_{2v} symmetry, while elastic scattering is larger by at least an order of magnitude for C_{3v} symmetry. These features are unchanged as the energy decreases to 0.5 keV. The dip seen in electron capture for C_{3v} symmetry is not present in elastic scattering. Third, at scattering angles near 180° , both elastic-scattering and electron-capture differential cross sections for C_{3v} symmetry drop sharply, suggesting the infrequent occurrence of actual head-on collisions. For C_{2v} symmetry, no significant characteristic is observed near this angle.

2. Comparison with the $H^+ + H$ system and the $e^+ + CH_4$ system

It is interesting to examine the similarity and dissimilarity of shapes of differential cross sections for different projectiles since, at least at high energy where the Born theory is valid, collision dynamics is known to be dependent on target properties only. For C_{3v} symmetry in which the H^+ projectile directly approaches the H atom, one may speculate that the dynamics are similar to those for $H^+ + H$ collisions. In comparison with differential cross sections obtained below 1 keV for $H^+ + H$ collisions at scattering angles less than 6° [23] (although the present results for C_{3v} symmetry at the same energies and angles show qualitatively similar oscillatory patterns below 2° for both elastic and electron-capture processes), details are markedly different in several respects. First, oscillations in the $H^+ + CH_4$ differential cross sections occur more frequently than in $H^+ + H$; for example, there are three oscillations in $H^+ + CH_4$ collisions at $1^\circ < \theta < 2^\circ$ and 500 eV but only one oscillation in $H^+ + H$ collisions in the same angle region. Second, the differential cross section for electron capture in $H^+ + CH_4$ collisions is far smaller (by two orders of magnitude) than that for elastic scattering, while these two processes are comparable in magnitude for $H^+ + H$. Third, at $\theta > 3^\circ$, the present results for $H^+ + CH_4$ show numerous oscillations, while oscillations for $H^+ + H$ appear to be damped within the model used. The origins of the oscillatory structures seen in $H^+ + H$ collisions have been thoroughly studied and are known to be due to combinations of interferences arising from (i) g (gerade)– u (ungerade) electronic symmetry, (ii) minimum (or maximum) in the difference between the two adiabatic potential curves concerned, and (iii) the multichannel effect. For the present $H^+ + CH_4$ collisions, an electron on a H atom combined with a $2p$

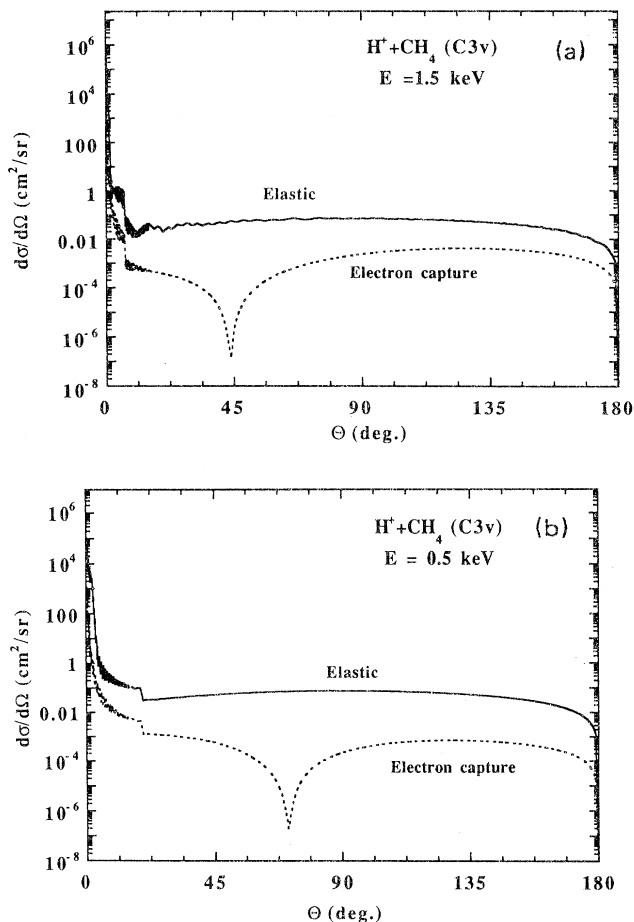


FIG. 4. (a) Differential cross section for C_{3v} at 1.5 keV. Solid line, elastic scattering; dashed line, electron capture. (b) Differential cross section for C_{3v} at 0.5 keV. Solid line, elastic scattering; dashed line, electron capture.

electron on the C atom forms a covalent bond, changing the character of the isolated H atom rather significantly and hence destroying completely the $g-u$ symmetry. This phenomenon may cause dissimilarity in differential cross sections, even though the molecular configuration of the collision appears to be similar in both cases. Multiple-scattering effects due to multiple centers in the CH_4 molecule (which translate into the difference in couplings) described below contribute at all energies, causing additional deviations from simpler $H^+ + H$ collisions.

Although the present collision system is expected to possess a somewhat remote relationship with the system for [positron (e^+) + CH_4] collisions, it may be interesting to compare them because the projectiles have the same charge state. Differential elastic cross sections for $e^+ + CH_4$ collisions were measured by Kaupila *et al.* [24] at 6 and 50 eV. Our elastic result at 11 keV (which corresponds to the same speed as that for 6-eV positrons) is isotropic over the entire angle region, except for the region near 0° , where a sharp forward peak can be observed [see Fig. 3(a) for an example]. For $e^+ + CH_4$ collisions, the situation is generally similar to the present case, with near-isotropic angle dependence and a large forward peak near 0° . However, one notable difference is the presence of one dip in the e^+ scattering at about 45° . This dip may arise from the interference effect among some partial waves; this interference is unique for ($e^+ / e^- + CH_4$) collisions because the lighter mass of the projectile causes a smaller number of partial waves (typically, $1 < 3$: f wave), to contribute than in proton impact (where a few thousand partial waves are required) in this velocity region. The present results for protons and those for ($e^+ + CH_4$) are conspicuously different from results for ($e^- + CH_4$) collisions [25], suggesting that the projectile-charge effect is more pronounced at this intermediate energy.

3. Multiple scattering

In the molecular configuration in which the projectile bisects an H—C—H bond angle in the molecule, the collision contributes little to small-angle scatterings because of weak interactions with the H atom. However, such a collision is expected to make a significant contribution to large-angle scatterings, because the projectile effectively interacts “twice” with the electron distribution from each H atom. We have examined this point by using the scattering S -matrix results, as discussed below.

C. Total cross sections

Total integrated cross sections are illustrated separately for C_{2v} and C_{3v} symmetries in Fig. 5. That of C_{2v} gradually increases as energy increases, reaching a maximum value of $1 \times 10^{-15} \text{ cm}^2$ at 300 eV, while that for C_{3v} is rather energy independent within the present energy region with a broad plateau value of $3 \times 10^{-17} \text{ cm}^2$ at 50 eV. Because of these characteristics for the two molecular orientations, the magnitudes of these two sets of cross sections appear to cross at even lower energy. Note that the total cross section for C_{3v} -face symmetry is

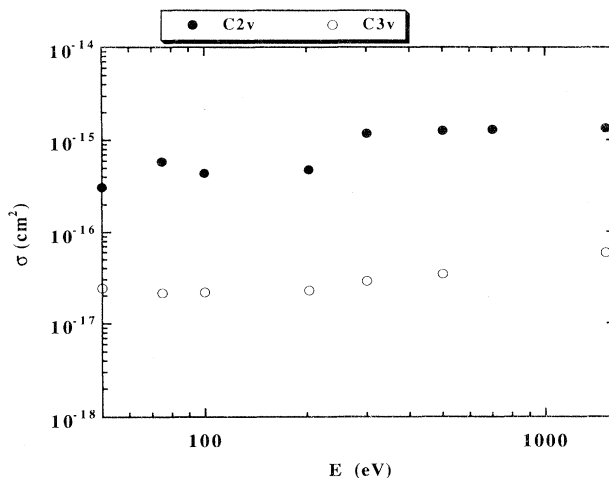


FIG. 5. Total electron-capture cross sections for C_{2v} and C_{3v} symmetries.

similar in magnitude to that for C_{2v} symmetry. The feature seen for C_{2v} symmetry is a reflection of a combination of two coupling peaks at $R=1.0$ and 5.5 a.u. Actual total-cross-section results that can be compared with experimental data should be ideally obtained by repeating the scattering calculations with a stepwise change of molecular orientation. A simple averaging of molecular orientation (taking the weighting factor for the molecular orientation into account) in the present result gives a rough estimate of about $1 \times 10^{-15} \text{ cm}^2$ at 1 keV, which compares fairly well with the experimental finding of $3 \times 10^{-15} \text{ cm}^2$ [10].

D. Interferences between different molecular orientations

Gao *et al.* [13] measured the differential cross section for electron capture from 0.01° to 1.0° at 1.5 keV. Their results, along with the present calculation for the system, are reproduced in Fig. 6. Agreement of the present individual results for C_{2v} and C_{3v} symmetries with the measurements is less satisfactory at larger and smaller scattering angles, respectively. In their experiment, Gao *et al.* actually observed the averaged differential cross section over all molecular geometries, not for a fixed well-identified geometry of a specific molecular configuration. Therefore, to properly compare our result with the measurement, we should employ an averaging procedure. By taking scattering amplitudes f_i from the two calculated molecular geometries and simply adding them coherently, we can obtain differential cross sections, viz., $d\sigma/d\Omega \sim |f_{C_{2v}} + f_{C_{3v}}|^2$, that may be compatible with the one in the experiment. Through this averaging procedure, we can examine the interference between different geometries in the collision dynamics. The result thus obtained is included in Fig. 6. Clearly, the averaged result improves the agreement with the measurement at all scattering angles below 1° . The averaged result is consistently similar to the C_{2v} result at angles below 0.4° , but the situation is reversed as the angle increases.

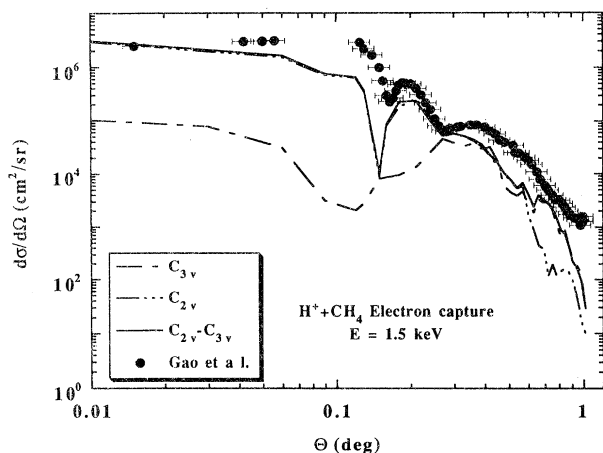


FIG. 6. Differential cross section from 0.01° to 1.0° at 1.5 keV. The solid line shows the averaged result, the dashed-dotted line the result for C_{3v} , and dashed three-dot line the result for C_{2v} . The \bullet symbols represent the experimental data of Gao *et al.* [13].

Differential cross sections for C_{2v} symmetry are uniformly larger than those for C_{3v} symmetry below 0.4° , but those for C_{2v} symmetry drop drastically at larger angles, while those for C_{3v} symmetry are isotropic. Only in the region where these two sets of cross sections become equal in magnitude is the consequence of the interference visible in this angular region. In fact, a small structure seen near 0.42° is the result of the interference of these two molecular symmetries. In other regions, one of the two configurations is overwhelmingly dominant; thus, it solely controls the dynamics.

E. Differential cross sections at low energies (<100 eV)

For low-energy collisions below 100 eV, more pronounced differences for C_{2v} and C_{3v} symmetries are apparent, reflecting an increasing sensitivity of dynamics to the molecular orientation. Differential cross sections at 20, 50, and 100 eV are illustrated for C_{2v} and C_{3v} symmetries for scattering angles 0° – 180° in Figs. 7(a)–7(c) 8(a)–8(c), respectively. Note that the present model may not offer accurate results below 50 eV, and hence the results for this energy region are considered to be qualitative. Some general features specifically observed in this particular energy regime are summarized here for C_{2v} and C_{3v} symmetries separately. The physical interpretation for these findings is essentially the same as in the case of high energy.

For C_{2v} symmetry: (i) The forward scattering both for elastic and electron capture at scattering angles less than 20° is dominant; (ii) numerous, small oscillations due to interferences (Stueckelberg-type) are seen at large angles $>40^\circ$; and (iii) elastic and electron-capture cross sections are of comparable magnitude. For C_{3v} symmetry: (i) Large and high-frequency oscillations are seen in the elastic cross section; (ii) at higher energies, these oscillations weaken and the scattering becomes more isotropic, i.e., a constant for a large range of scattering angles; and (iii)

large rainbow dips are observed in electron-capture cross sections at several scattering angles at lower energies, and the number of dips decrease as the energy increases. To summarize the differences: (i) Above 20 eV, the electron-capture cross section becomes larger than that for elastic scattering at $\theta \geq 40^\circ$ for C_{2v} symmetry. For C_{3v} symmetry, the elastic-scattering and electron-capture processes approach each other somewhat at $\theta \geq 150^\circ$, but their magnitudes are not inverted; (ii) the behavior of differential cross sections for C_{2v} and C_{3v} symmetries is markedly distinctive. For C_{2v} symmetry, differential cross sections for electron capture show a few oscillations at large-angle scattering for $\theta \gtrsim 50^\circ$. In contrast, for C_{3v} symmetry, the numerous oscillations in the entire angle region are obvious. This observation is conspicuously opposite to that for results at high energies of $E > 0.5$ keV. Note that general shapes for both differential cross sections for C_{3v} -face symmetry are similar to those for C_{2v} symmetry.

In order to understand the scattering mechanisms clearly, scattering S -matrix elements for C_{2v} and C_{3v} symmetries are plotted in Figs. 9(a) and 9(b) as a function of partial wave l at 20 and 50 eV. For both C_{2v} and C_{3v} symmetries, S -matrix elements apparently exist only in the l region, where the corresponding couplings are effective, i.e., inside $7.5a_0$ and $4.5a_0$, for C_{2v} and C_{3v} , re-

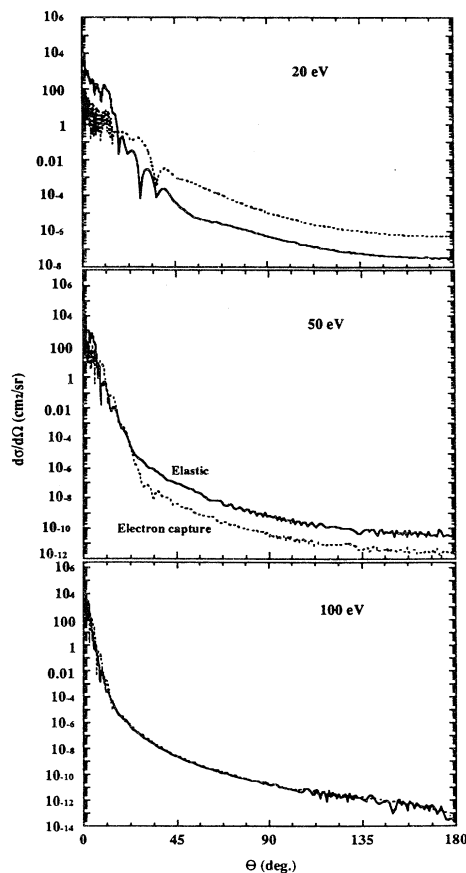


FIG. 7. Differential cross section for C_{2v} : (a) 20 eV, (b) 50 eV, (c) 100 eV.

spectively (see also Fig. 2, coupling matrix elements). Because of the influence of the first peak at $1.0a_0$ for C_{2v} for the dynamics, general shapes and structures of the S -matrix element for C_{2v} are quite different from those for C_{3v} . For C_{3v} , a good combination of the strength of the coupling and energy separation between two adiabatic potential curves at around $4a_0$ makes the transition quite efficient at this point, while the combination makes it rather inefficient inside this R region, resulting in smaller S -matrix values at smaller l . In contrast, for C_{2v} , because of the effectiveness of the inside coupling at $1.0a_0$, values of the S -matrix element increase as l becomes smaller. These features reflect two distinct coupling schemes for C_{2v} and C_{3v} , namely, that for C_{2v} , the coupling at $1.0a_0$ becomes more efficient than the outer coupling at $6a_0$, while for C_{3v} , the pure Demkov-type mechanism is the sole mechanism. As the collision energy increases, the number of oscillations in the S -matrix elements decreases because of the shorter interaction times, and also their magnitude for C_{3v} approaches substantially decreases. Note again that the S -matrix elements for C_{3v} -face symmetry are close in nature to those of C_{2v} symmetry.

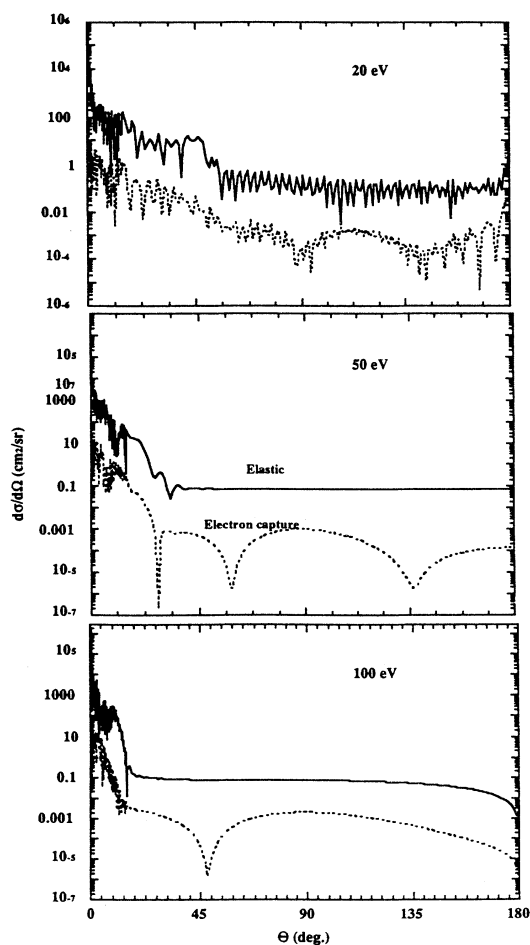


FIG. 8. Differential cross section for C_{3v} : (a) 20 eV, (b) 50 eV, (c) 100 eV.

F. Dissociation fragmentations

Although it is not our main aim in the present study to undertake a detailed examination of the fragmentations that occur after electron capture, nevertheless it is interesting to consider other reaction channels in which the methane target or its positive ion undergoes subsequent fragmentation, and some remarks on the fragmentation are warranted. In the low-keV region, the collision energy range that is studied here, single-electron capture is the dominant process, and ionization and double-electron-capture processes are considered to be of negligible importance. As the present result shows, the CH_4^+ ion that is produced is mostly in its ground electronic state, which is a degenerate Jahn-Teller state that forms a stable molecular ion of a distorted geometry. As Figs. 1(a) and 1(b) show, the $(CH_4 + H^+)$ asymptote lies below that of $(H + CH_4^+)$. Relaxation of the CH_4 geometry, not considered in the present calculations, reverses this situation, so that the H atom asymptote lies 0.6 eV below that of H^+ at equilibrium. Because in the energy region considered, the collision time is about 10^{-15} s, whereas more than 10^{-13} s would be required for a vibrational period, such nuclear relaxation processes do not have sufficient time to occur. Thus, the present results, obtained with a fixed methane conformation, are more real-

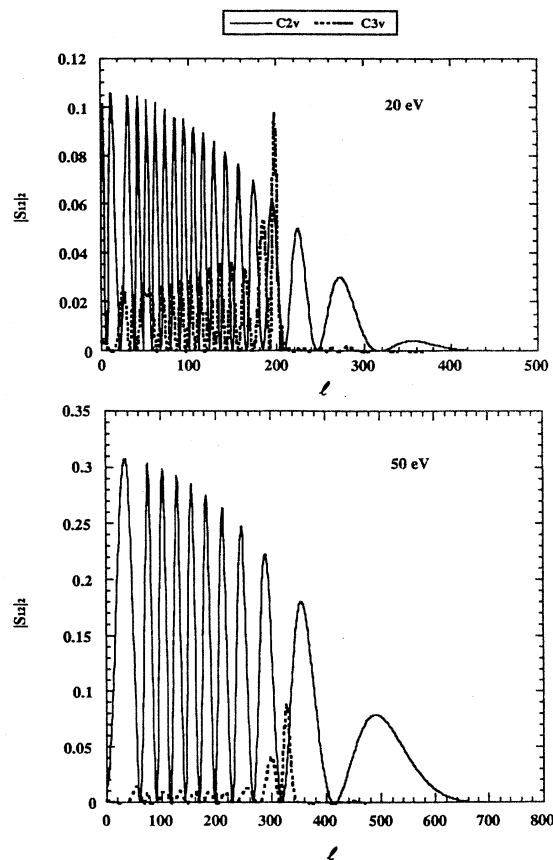


FIG. 9. Scattering S -matrix element for C_{2v} and C_{3v} at (a) 20 eV and (b) 50 eV.

istic. The combination of lowest-energy fragments involving two hydrogen atoms and/or ions is found to be $(\text{CH}_3^+ + \text{H} + \text{H})$, with an energy that is 1.2 eV above that of the $(\text{CH}_4^+ + \text{H})$ limit. In other words, the dissociation energy of CH_4^+ is significantly smaller (1.2 eV) than that of neutral methane (4.4 eV). Thermodynamically, the distinction arises because the ionization potential of methane (12.99 eV) is 3.2 eV larger than that for CH_3 (9.843 eV). In molecular-orbital (MO) terms, this relationship is easily understandable, because the highest occupied molecular orbital (HOMO) in each case is greatly stabilized by the bonding of hydrogen atoms to carbon, and thus the orbital energy of the HOMO is notably lower for CH_4 than for CH_3 , causing the CH_3 system's ionization potential to be smaller than for methane itself. The next most stable set of fragments is $(\text{CH}_3^+ + \text{H} + \text{H}^+)$, whose energy is 5.0 eV above the lowest $(\text{CH}_4^+ + \text{H})$ limit. This limit can be reached from the second most stable set of fragments, $(\text{CH}_4 + \text{H}^+)$, by removing an H atom from the methane system. The dominant breakup pathway of the CH_4^+ ion is known to be



leading to a CH_3^+ ion and a neutral H atom. This CH_3^+ ion is unstable and is likely to break into smaller fragments through predissociation.

If the CH_4^+ ion produced is in one of the electronic excited states with a rovibrationally excited level, then a large number of breakup pathways become available for producing a variety of fragments of neutral and ionic species, such as $(\text{CH}_3 + \text{H}^+)$ and $(\text{CH}_2^+ + \text{H}^+ + \text{H})$, which are likely to be rovibrationally excited species. These unstable species undergo further breakup. In high-density gaseous or condensed media, these species undergo a series of chemical chain reactions. Knowledge of the yields of these fragments is essential for modeling in astrophysics, plasma chemistry, and radiation chemistry. However, this type of knowledge is still far from

complete, and a systematic study of molecular fragmentation is urgently needed.

IV. SUMMARY

A theoretical study of elastic and electron-capture processes in collisions of H^+ ions with CH_4 molecules in the energy range from 20 eV to 1.5 keV was carried out for two distinct molecular orientations, the C_{2v} and C_{3v} symmetries, by using a three-channel molecular-orbital method within a quantum-mechanical formalism. A limited study for C_{3v} -face symmetry was also carried out to examine the effect of molecular orientation. Collision dynamics for C_{2v} and C_{3v} symmetries were found to be effective in two nonoverlapping scattering-angle regions. Hence, the interference arising from these two molecular configurations occurs only in very narrow regions of the scattering angle. However, weak but unambiguous structures in differential cross sections arising from the interference are observed. The differential cross section for electron capture at 1.5 keV that takes interference into account was found to be in good agreement with the measurement by Gao *et al.* [13]. The integrated cross section for electron capture is also in reasonable accord with the measurement, with a magnitude of $1 \times 10^{-15} \text{ cm}^2$ at 1 keV. We plan to extend the present study to examine explicitly the fragmentation products at 1 keV and will report the results elsewhere.

ACKNOWLEDGMENTS

M.K. is grateful to Dr. Kauppila for useful discussions on the $(e^+ + \text{CH}_4)$ experiment. The work was supported in part by the U.S. Department of Energy, Office of Energy Research, Office of Health and Environment Research, under Contract No. W-31-109-Eng-38; and by the Deutsche Forschungsgemeinschaft in the form of a Forschergruppe grant. Financial support of the Fonds der Chemischen Industrie is also hereby gratefully acknowledged (Y.L., G.H., and R.J.B.).

-
- [1] M. Kimura and N. F. Lane, *Advanced Atomic Molecular Physics*, edited by D. R. Bates and B. Bederson (Academic, New York, 1989), Vol. 26, p. 79.
- [2] W. Fritsch and C. D. Lin, *Phys. Rep.* **202**, 1 (1991).
- [3] M. Kimura, *Phys. Rev. A* **32**, 802 (1985).
- [4] R. Shingal and C. D. Lin, *Phys. Rev. A* **40**, 1302 (1989).
- [5] W. Fritsch, *Phys. Rev. A* **46**, 3910 (1992).
- [6] M. B. Shah and H. B. Gilbody, *J. Phys. B* **11**, 121 (1978).
- [7] D. Cicić, D. Dijkkamp, E. Vliegad, and F. J. de Heer, *J. Phys. B* **18**, 4745 (1985).
- [8] R. Hoekstra, Ph.D. thesis, University of Groningen, 1990 (unpublished).
- [9] K. Kobayashi, M. Tsuchiya, T. Oshima, and H. Yanagawa, *Origins Life* **20**, 99 (1990).
- [10] J. H. Birely and R. J. McNeil, *J. Chem. Phys.* **56**, 2189 (1972).
- [11] M. Eliot, *J. Phys. (Paris)* **38**, 21 (1977).
- [12] I. Ben-Itzhak, K. D. Carnes, S. G. Ginther, D. T. Johnson, P. J. Norris, and O. L. Weaver, *Phys. Rev. A* **47**, 3748 (1993).
- [13] R. S. Gao, L. K. Johnson, C. L. Hakes, K. A. Smith, and R. F. Stebbings, *Phys. Rev. A* **41**, 5929 (1990).
- [14] G. Niedner, M. Noll, and J. P. Toennies, *J. Chem. Phys.* **87**, 2067 (1987).
- [15] B. Friedrich, G. Niedner, M. Noll, and J. P. Toennies, *J. Chem. Phys.* **87**, 5256 (1987).
- [16] Y. N. Chiu, B. Friedrich, W. Maring, G. Niedner, M. Noll, and J. P. Toennies, *J. Chem. Phys.* **88**, 6814 (1988).
- [17] V. G. Anicich and W. T. Huntress, Jr., *Astrophys. J. Suppl. Ser.* **62**, 553 (1986).
- [18] R. J. Buenker and S. D. Peyerimhoff, *Theor. Chim. Acta* **35**, 33 (1974); **39**, 217 (1975); R. J. Buenker, *Intern. J. Quantum Chem.* **29**, 435 (1986).
- [19] D. B. Knowles, J. R. Alvarez-Corrado, G. Hirsch, and R. J. Buenker, *J. Chem. Phys.* **92**, 585 (1990).
- [20] S. Huzinaga, *J. Chem. Phys.* **42**, 1293 (1965).

- [21] T. H. Dunning, Jr., *J. Chem. Phys.* **53**, 2823 (1970).
- [22] R. E. Olson and F. T. Smith, *Phys. Rev. A* **3**, 1607 (1971).
- [23] M. Kimura, Ph.D. thesis, University of Alberta, 1981 (unpublished); see also R. Schinke and H. Kruger, *J. Phys. B* **9**, 2469 (1976).
- [24] W. E. Kauppila, L. Dou, C. K. Kwan, D. Przybyla, S. J. Smith, and T. S. Stein, *XVIII International Conference on the Physics of Electronic and Atomic Collisions*, edited by T. Andersen, B. Fastrup, F. Folkmann, and H. Knudsen (IFA, University of Aarhus, Aarhus, 1993), Vol. II, p. 414.
- [25] R. Müller, L. Kung, K.-H. Kochem, W. Sohn, and H. Ehrhardt, *J. Phys. B* **18**, 3971 (1985).